TOP-PASS: A processing algorithm to reduce 2D PASS acquisition time

Michael C. Davis, Kimberly M. Shookman, Jacob D. Sillaman, Philip J. Grandinetti*

Department of Chemistry, The Ohio State University, 120 W. 18th Avenue, Columbus, Ohio 43210-1173

Abstract

A slow speed MAS spectrum contains a pattern of spinning sideband resonances separated by integer multiples of the rotor frequency and centered about an isotropic frequency. The 2D signal acquired in a two-dimensional Phase Adjusted Spinning Sideband (PASS) experiment correlates this slow speed MAS spectrum, obtained in the direct dimension, to an indirect dimension spectrum containing the same pattern of spinning sideband resonances centered about a frequency of zero. An affine transformation is used to convert the acquired 2D PASS signal into a 2D signal that correlates a spectrum of pure isotropic frequencies to a spectrum of spinning sideband resonances with no isotropic frequency contributions. The conventional affine transform applied to 2D PASS consists of an active shear of the signal parallel to the indirect time domain coordinate followed by a passive scaling of the indirect time domain coordinate. Here we show that an alternative affine transform, previously employed in the Two-dimensional One Pulse (TOP) experiment, can be employed to create the same 2D signal correlation with an enhanced spectral width in the anisotropic (spinning sideband) dimension. This enhancement can provide a significant reduction in the minimum experiment time required for a 2D PASS experiment, particularly for spectra where the individual spinning sideband patterns are dispersed over a wider spectral range than the isotropic resonance frequencies. The TOP processing consists of an active shear of the signal parallel to the direct time domain, followed by an active shear of the signal parallel to the new indirect time domain coordinate followed by a passive scaling of the new direct time domain coordinate. A theoretical description of the affine transformation in the context of 2D PASS is given along with illustrative examples of ^{29}Si in Clinoenstatite and ^{13}C in L-Histidine.

1. Introduction

Frequency anisotropy in magnetic resonance spectroscopy is a rich source of detail concerning structure and dynamics at the macroscopic level down to the molecular level. At the macroscopic level these anisotropies can occur as a result of inhomogeneities in the external magnetic field, variations in magnetic susceptibilities, or through the intentional use of magnetic field gradients as in magnetic resonance imaging. At the molecular level frequency anisotropy arises through magnetic dipolar couplings amongst nuclei and through interactions of the nuclear multipole moments with surrounding electrons. While the manifestation of these molecular level anisotropies in solution state NMR is primarily through relaxation, its effects are seen directly in solid-state NMR spectra as the powder pattern lineshape.

Early in the history of NMR it was realized that inhomogeneous anisotropic broadenings can

*Corresponding author

URL: http://www.grandinetti.org (Philip J. Grandinetti)

be removed through sample rotation[1–3]. In solution state NMR, sample rotation is a standard approach to average away broadenings from magnetic field inhomogeneities[1], while magic-angle sample spinning (MAS)[2, 3] has become a popular and routine method in solid-state NMR for eliminating second-rank anisotropic broadenings, particularly when combined with the sensitivity enhancement of cross-polarization (CP/MAS)[4, 5]. With sample rotation, the inhomogeneous lineshape breaks up into a set of spinning sidebands centered about a centerband lineshape and spaced at integer multiples of the spinning frequency. As the spinning frequency is increased the intensities of the spinning sidebands are reduced and transferred into the centerband. In the limit of infinite spinning speed only the centerband frequency remains.

A few years after the introduction of CP/MAS, Herzfeld and Berger[6] developed an approach for analyzing the sideband intensities in a slow speed MAS spectrum to obtain the same details about the anisotropic spin interactions as found in the static powder pattern lineshape. With the introduction of two-dimensional NMR spectroscopy[7], a number of approaches have been designed to correlate a high or infinite speed MAS spectrum with either the static[8–13], slow speed MAS spectrum[14–18] or only spinning sideband intensities[19, 14–18]. One of the more popular approaches is the elegant Phase Adjusted Spinning Sidebands (PASS) experiment of Dixon[19]. While 2D PASS[16] robustly correlates isotropic frequencies to spinning sideband patterns, it has a drawback that experiment times can become lengthy when spectra contain sites having a large number of spinning sidebands. In such situations, the sampling rate in the indirect dimension is increased or the spinning speed is increased. The latter approach, however, could result in a loss of sideband information from other sites with smaller anisotropies. Here, we describe an alternative approach for processing 2D PASS signals, based on the TOP experiment[20–22], which increases the spectral width in the anisotropic (spinning sideband) dimension without increasing the sampling rate in the indirect (rotor pitch) dimension (or even changing the spinning speed). We refer to this combination of TOP processing applied to the 2D PASS signal as the TOP-PASS experiment. This new approach can provide a significant reduction in the minimum experiment time required for a 2D PASS experiment, particularly for samples with large anisotropies as well as those simply having long relaxation times.

2. Experimental

NMR experiments on Clinoenstatite, $MgSiO_3$, were performed on a Bruker Avance operating at a field strength of 9.4 Tesla corresponding to an operating frequency of 79.576 MHz for ^{29}Si with a 4 mm Bruker MAS probe spinning at 1000 ± 2 Hz using ^{29}Si rf field strength of 94 kHz. NMR experiments on L-Histidine were performed on a hybrid Tecmag Apollo-Chemagnetics CMX II NMR spectrometer operating at a field strength of 9.4 Tesla, corresponding to an ^{13}C NMR frequency of 100.605 MHz and a ^{1}H NMR frequency of 400.068 MHz, and using a 4 mm Chemagnetics double resonance MAS probe spinning at 1500 ± 2 Hz with a ^{1}H rf field strength of 83 kHz for initial excitation and TPPM decoupling, a ^{1}H-^{13}C cross-polarization contact rf field strength of 104.17 kHz and contact time of 1.1 ms. An exponential apodization of 50 Hz in the direct dimension and 100 Hz in the indirect dimension was applied to all 2D datasets. L-Histidine monochloride monohydrate was obtained from Sigma Aldrich and used without further purification. The acquisition time for a single 2D PASS cross-section in the indirect dimension for Clinoenstatite and L-Histidine was 9 hours and 1.5 hours, respectively.

3. Results and Discussion

3.1. Bloch Decay MAS

The first-order contribution of the nuclear shielding to the NMR frequency for a single crystallite as a function of rotor angle and phase can be expanded in a Fourier series[23] as

$$\Omega_{\sigma}^{(1)}(\theta_R,\phi_R) = \varpi_0(\theta_R,\alpha,\beta) + \sum_{m\neq 0} \varpi_m(\theta_R,\alpha,\beta) e^{im(\phi_R+\gamma)}, \quad (1)$$

where θ_R is the rotor angle, ϕ_R is the rotor phase, α, β, and γ are the Euler angles between the rotor coordinate frame and the crystallite coordinate frame. In the simple Bloch decay MAS experiment the signal phase as function of time, t, where $\phi_R(t) = \omega_R t + \chi_R$, is

$$\begin{aligned}\Phi(t) &= \int_0^t \Omega_{\sigma}^{(1)}(\theta_R,\phi_R(t'))\,dt' \\ &= W_0\, t \, + \sum_{m\neq 0} W_m e^{im(\chi_R+\gamma)}\left[e^{im\omega_R t} - 1\right],\end{aligned} \quad (2)$$

where χ_R is the initial rotor phase, and we define

$$W_0 = \varpi_0(\theta_M,\alpha,\beta), \quad (3)$$

and

$$W_m = \frac{\varpi_m(\theta_M,\alpha,\beta)}{im\omega_R}. \quad (4)$$

Here $\theta_M = \cos^{-1}(1/\sqrt{3})$. One can show[23] that the Bloch decay MAS signal is given by

$$\mathfrak{s}_B(\alpha,\beta,t,\chi_R) = \mathfrak{s}^e(t)\, e^{iW_0 t} \times \sum_{N_1,N_2} A_{N_1} A^*_{N_2} e^{-iN_1\omega_R t} e^{i(N_2-N_1)(\chi_R+\gamma)}, \quad (5)$$

where

$$A_N = \frac{1}{2\pi}\int_0^{2\pi} \exp\left\{ i \sum_{m\neq 0} W_m e^{im\Theta}\right\} e^{iN\Theta} d\Theta, \quad (6)$$

and $\mathfrak{s}^{\mathrm{e}}(t)$ represents the envelope function due to the relaxation. A partial averaging of the Bloch decay signal over the angle γ eliminates the dependence on the initial rotor phase, χ_R, yielding

$$\langle \mathfrak{s}_B(\alpha,\beta,t)\rangle_{\gamma} = \mathfrak{s}^e(t)\, e^{iW_0 t} \sum_N |A_N|^2 e^{-iN\omega_R t}. \quad (7)$$

The Bloch decay MAS signal from all crystallites, $\mathcal{S}_B(t)$, is then given by

$$\begin{aligned}\mathcal{S}_B(t) &= \int_0^{2\pi} d\alpha \int_0^{\pi} \sin\beta\, d\beta\, \langle \mathfrak{s}_B(\alpha,\beta,t)\rangle_{\gamma} \\ &= \mathfrak{s}^e(t)\, e^{iW_0 t} \sum_N I_N e^{-iN\omega_R t},\end{aligned} \quad (8)$$

where

$$I_N = \int_0^{2\pi} d\alpha \int_0^{\pi} \sin\beta\, d\beta\, |A_N|^2. \quad (9)$$

Notice that W_0 during MAS is only dependent on isotropic frequency contributions, whereas the spinning sideband intensities, I_N, are only dependent on anisotropic frequency contributions.

3.1.1. TOP

One can rewrite Eq. (8) in the form

$$\mathcal{S}(t_1,t_2) = \mathfrak{s}^{\mathrm{e}}(t_2) e^{iW_0 t_2} \sum_N I_N e^{-iN\omega_R t_1}, \quad (10)$$

and visualize the 1D Bloch decay MAS signal from a rotating sample as a signal filling a 2D t_1–t_2 coordinate system, as illustrated in Fig. 1. Note that

$$\mathcal{S}_B(t_1 + nt_R, t_2) = \mathcal{S}_B(t_1,t_2), \quad (11)$$

where $t_R = 2\pi/\omega_R$ and n is an integer. The significance of this coordinate system is that the isotropic frequency contributions are removed along the t_1 dimension, and the anisotropic frequency contributions are removed along the t_2 dimension. This coordinate system is particularly useful for understanding a number of important solid-state NMR experiments for manipulating rotary echoes and

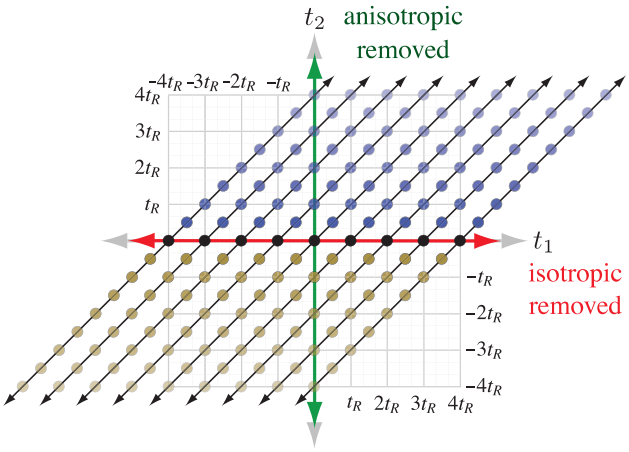

Figure 1: Solid circles and arrows represent the sampling trajectory of the 1D Bloch decay MAS signal (blue circles) and its complex conjugate signal (brown circles) in the t_1–t_2 coordinate system. The slope of the sampling trajectory in the t_1-t_2 coordinate system is 1. Identical signal run parallel, separated by t_R in t_1 and t_2, respectively. Only anisotropic frequency contributions are present along the t_1 dimension, and only isotropic frequency contributions are present along the t_2 dimension.

their associated spectral spinning sidebands. Probably the simplest of these is the Two-dimensional One Pulse (TOP) processing approach [20–22], which samples the 2D signal of Eq. (10) using identical 1D Bloch decay signals running parallel to each other and separated by t_R in both t_1 and t_2, as shown in Fig. 1.

In the TOP approach, one first generates a pseudo-2D signal, $\mathcal{S}_{\text{top}}(\epsilon, t)$, in a ϵ–t coordinate system from the 1D Bloch decay (or rotor synchronized Hahn echo) signal, $\mathcal{S}_B(t)$. This is illustrated in Fig. 2A, where a sampling of $\mathcal{S}_{\text{top}}(\epsilon, t)$ for positive and negative values of ϵ is generated using the relationship

$$\mathcal{S}_{\text{top}}(\epsilon_n = n2\pi/\omega_R, t) = \mathcal{S}_B(t), \qquad (12)$$

for a range of positive and negative integer n values. The 2D signal constructed in this manner has no decay from relaxation along the ϵ dimension. This 2D signal produces a pure absorption mode

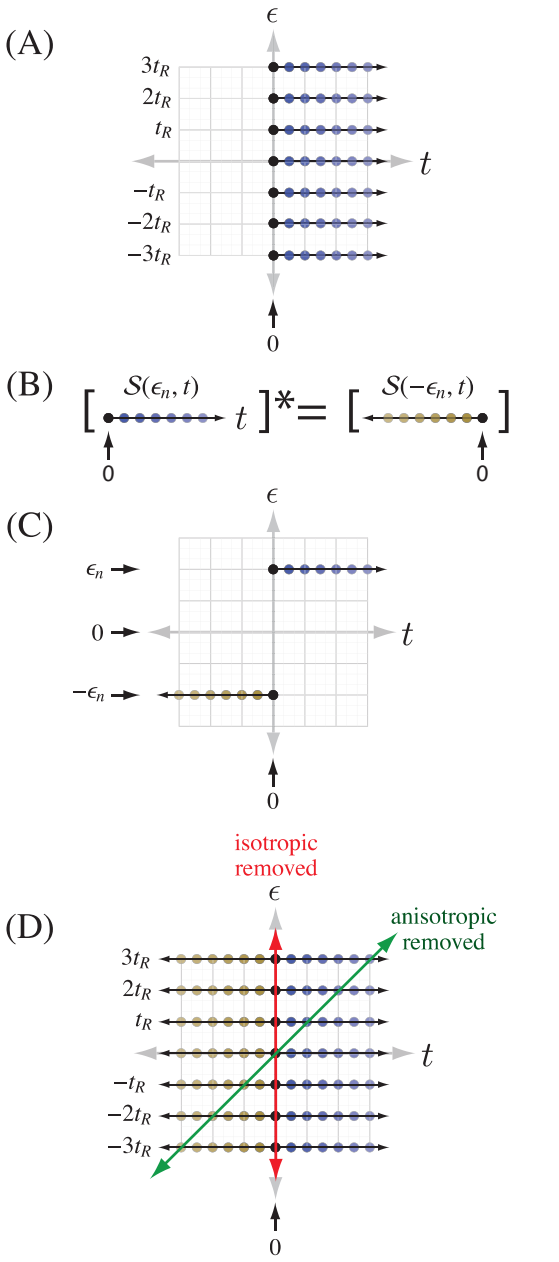

Figure 2: Scheme for generating the pseudo-2D signal for TOP processing from the 1D Bloch decay signal in a rotating sample. (A) Identical Bloch decay signal are laid down in a coordinate system at integer multiples of the rotor period along the ϵ dimension. (B) The complex conjugate of the 1D Bloch decay signal is used to generate a Bloch decay signal going backward in time. (C) Identical complex conjugate Bloch decay signals are placed in opposite quadrant in the t–ϵ coordinate system. (D) The TOP signal before application of the affine transformation.

2D spectrum since it is generated for positive and negative values of ϵ, as illustrated in Fig. 2A. If desired, a full sampling of the TOP signal in all four quadrants can be generated using the complex conjugate of the Bloch decay signal, $\mathcal{S}^*_B(t)$, as illustrated in Fig. 2B and 2C. In the generated 2D signal, $\mathcal{S}_{\text{top}}(\epsilon, t)$, acquired as a function of ϵ and t_2, the anisotropic frequency contributions are refocused into a echo along the line $\epsilon + t_1 = 0$, and the isotropic frequency contribution is refocused along $t = 0$, as shown in Fig. 2D.

After the 2D signal, $\mathcal{S}_{\text{top}}(\epsilon, t)$, is created, an affine transformation, as illustrated in Fig. 3, is applied to separate the isotropic and anisotropic frequency contributions into orthogonal dimensions. For the TOP signal this is performed as a double shear, starting with a shear parallel to the t coordinate with a shear ratio of $\kappa_t = -1$, followed by a shear parallel to the t'_2 coordinate with a shear ratio of $\kappa_{t'_2} = 1$, according to

$$\begin{aligned}\begin{bmatrix} t_2 \\ t_1 \end{bmatrix} &= \underbrace{\begin{bmatrix} 1 & 1 \\ 0 & 1 \end{bmatrix}}_{\boldsymbol{K}_{t'_2}} \underbrace{\begin{bmatrix} 1 & 0 \\ -1 & 1 \end{bmatrix}}_{\boldsymbol{K}_t} \begin{bmatrix} \epsilon \\ t \end{bmatrix} \\ &= \begin{bmatrix} 0 & 1 \\ -1 & 1 \end{bmatrix} \begin{bmatrix} \epsilon \\ t \end{bmatrix}. \end{aligned} \tag{13}$$

The application of this affine transformation to $\mathcal{S}_{\text{top}}(\epsilon, t)$ yields the TOP[22] signal in Eq. (10) whose Fourier transform yields a 2D spectrum correlating isotropic and anisotropic frequencies. Prior to the final 2D Fourier transformation, a matched-filter apodization can be applied along the t_2 (isotropic) dimension to improve sensitivity. Any apodization along the t_1 (anisotropic, sideband) dimension, however, is applied entirely for cosmetic reasons, creating a purely artificial line broadening of the sideband resonances. Most importantly, note that the application of this affine transformation to the original digital sampling

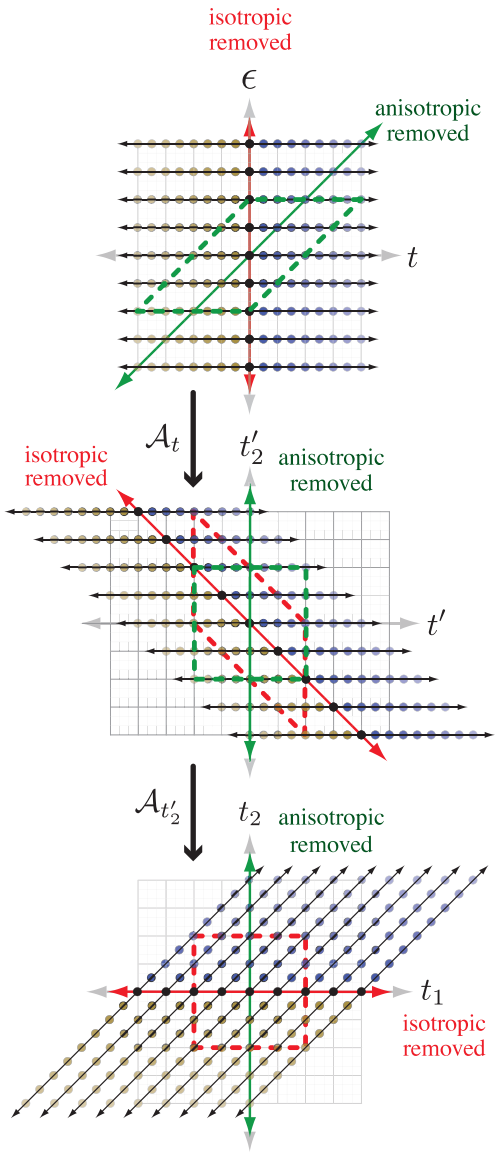

Figure 3: TOP transformation of $\mathcal{S}(\epsilon, t)$ into a 2D signal that correlates isotropic and anisotropic frequencies. An affine transformation, $\mathcal{A}_t$, consisting of a shear parallel to t, creates a 2D signal with anisotropic frequencies refocused along the t'_2 axis and the isotropic frequences refocused along $t + \epsilon = 0$. The green dashed line in the top figure represents the passive affine transformation of the 2D coordinate system to create a time coordinate, t'_2, along which the 2D signal is unaffected by the anisotropic frequency contributions. After $\mathcal{A}_{t'_2}$, a shear parallel to t'_2, a 2D signal with anisotropic frequencies refocused along the t_2 axis and isotropic frequencies is refocused along t_1 is obtained. The red dashed line in the middle figure represents the passive affine transformation of the 2D coordinate system to create a time coordinate, t_1, along which the 2D signal is unaffected by the isotropic frequency contributions.

rates, $\Delta\epsilon$ and Δt, yields transformed sampling rates of $\Delta t_2 = \Delta\epsilon = t_R$ and $\Delta t_1 = \Delta t$, respectively, after the double shear transformation.

In Fig. 4 is an example of the application of the TOP processing applied to a 2D signal, $\mathcal{S}_{\rm top}(\epsilon, t)$, constructed from the ^{29}Si NMR Hahn echo signal of polycrystalline Clinoenstatite. Clinoenstatite has two inequivalent tetrahedrally coordinated (i.e., $Q^{(2)}$) silicon sites, resolved at -85.2 ppm and -82.8 ppm in the isotropic dimension, and exhibit similar nuclear shielding anisotropies, as expected[24, 25], in the sideband dimension.

A limitation of TOP processing applied to a 1D Bloch decay (or rotor synchronized Hahn echo) MAS signal is that the spectral width in ω_2, the isotropic frequency dimension, is limited to integer divisors of the rotor frequency. This cannot be easily corrected by increasing the rotor frequency since it also reduces the information content in the sideband intensities. Nonetheless, TOP processing applied to a 1D Bloch decay has a number of added advantages, particularly when applied to half-integer quadrupolar nuclei[22] where its main strength lies in the rapid interpretation of MAS signals. The experimental simplicity of TOP processing applied to a 1D Bloch decay makes it a compelling method, and it is surprising that it has not been more widely utilitized.

3.1.2. 2D PASS

Generally, the NMR signal in a rotating sample can be manipulated into a number of desirable forms by applying a series of π pulses between the initial excitation pulse and the start of signal acquisition. In the PASS experiment [19, 16], a time coordinate is defined where the initial excitation pulse is applied at $t = -T$ and signal acquisition begins at $t = 0$. Between the initial excitation pulse and signal acquisition are Q π-pulses, applied at times $-T + \tau_1, -T + \tau_2, \ldots, -T + \tau_Q$. The signal phase at $t = 0$, a duration of $\tau_{Q+1} = T$ after the initial excitation pulse, is given by

$$\begin{aligned}
\Phi_Q(t=0) &= (-1)^Q \sum_{q=0}^{Q} (-1)^q \int_{-T+\tau_q}^{-T+\tau_{q+1}} \Omega(t')dt', \\
&= W_0 \left[T - 2(-1)^Q \sum_{q=1}^{Q} (-1)^q \tau_q \right] \\
&+ \sum_{m\neq 0} W_m e^{im(\chi_R+\gamma)} \\
&\times \left[1 - 2(-1)^Q \sum_{q=1}^{Q} (-1)^q e^{im\theta_q} e^{-im\theta_T} - (-1)^Q e^{-im\theta_T} \right],
\end{aligned} \tag{14}$$

where $\tau_0 = 0$, $\theta_T = \omega_R T$, and $\theta_q = \omega_R \tau_q$.

In the PASS experiment [19, 26] the timings of the Q π pulses are manipulated so the signal phase at $t = 0$ has a form

$$\begin{aligned}
&\Phi_{\rm pass}(\epsilon, t=0) = \\
&\quad W_0 [\ 0\ ] + \sum_{m\neq 0} W_m e^{im(\chi_R+\gamma)} \left[1 - e^{-im\omega_R\epsilon} \right],
\end{aligned} \tag{15}$$

where ϵ is a function of the Q π pulse timings. Evolving forward from $t = 0$ the PASS signal phase then becomes similar to the Bloch decay MAS signal

$$\begin{aligned}
&\Phi_{\rm pass}(\epsilon, t) = \\
&\quad W_0\, t + \sum_{m\neq 0} W_m e^{im(\chi_R+\gamma)} \left[e^{im\omega_R t} - e^{-im\omega_R\epsilon} \right],
\end{aligned} \tag{16}$$

with the important exception that ϵ is non-zero and can be varied independent of t. The PASS approach for obtaining the signal phase of Eq. (15) comes from equating Eqs. (14) and (15) to obtain the PASS equations:

$$\theta_T - 2(-1)^Q \sum_{q=1}^{Q} (-1)^q \theta_q = 0, \tag{17}$$

and

$$\begin{aligned}
&e^{-im\Theta} = \\
&\quad 2(-1)^Q \sum_{q=1}^{Q} (-1)^q e^{im\theta_q} e^{-im\theta_T} + (-1)^Q e^{-im\theta_T},
\end{aligned} \tag{18}$$

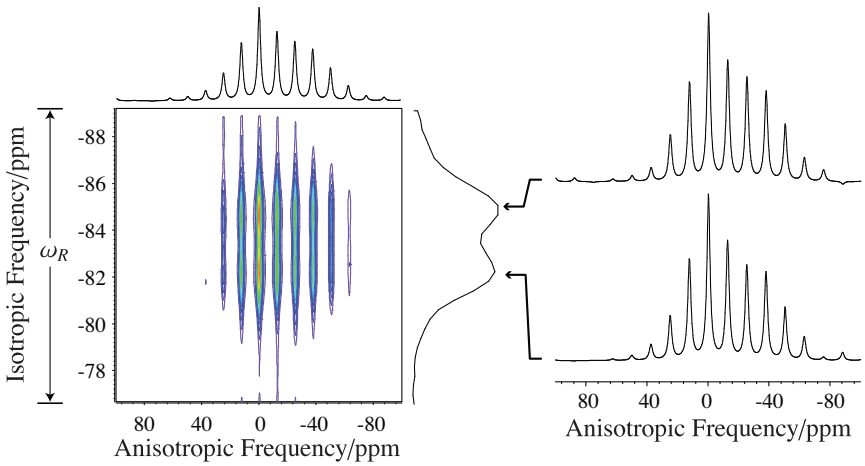

Figure 4: Application of TOP processing to a ^{29}Si NMR rotor synchronized Hahn echo signal of Clinoenstatite. Isotropic frequencies are referenced to TMS. Contour levels are plotted from 5%-100% in increments of 5% of the maximum intensity.

where $\Theta = \omega_R \epsilon$. Levitt and coworkers[16] suggested a five π pulse ($Q = 5$) 2D PASS experiment, of constant duration T, with $\theta_T = 2\pi$, and obtained the equations

$$2\sum_{q=1}^{5}(-1)^q\theta_q + 2\pi = 0, \qquad (19)$$

and

$$-2\sum_{q=1}^{5}(-1)^q e^{im\theta_q} - 1 = e^{-im\Theta}, \quad \text{for } m = 1, 2. \qquad (20)$$

These equations can be solved numerically for the π pulse timings shown in Fig. 5 and are tabulated elsewhere[16].

The phase of Eq. (16) leads to a PASS signal[23], when averaged over the crystallite angles, of the form

$$\mathcal{S}_{\text{pass}}(\epsilon, t) = e^{iW_0 t}\sum_N I(N)e^{-iN\omega_R(t+\epsilon)}. \qquad (21)$$

The 2D PASS signal, just like the Bloch decay MAS signal, can be used to fill the 2D signal in a ϵ–t coordinate system, as shown at the top of Fig. 6.

In the case of PASS, a single shear parallel to the ϵ coordinate with a shear ratio of $\kappa_\epsilon = -1$ followed

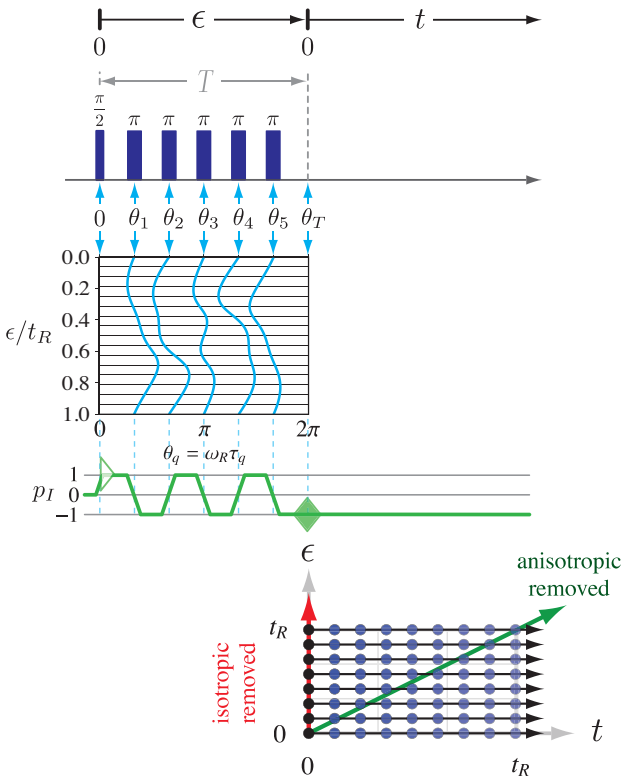

Figure 5: Pulse sequence and timings for the five π pulse constant time 2D PASS experiment of Antzutkin et al.[16]. Here, ω_R is the rotor spinning frequency.

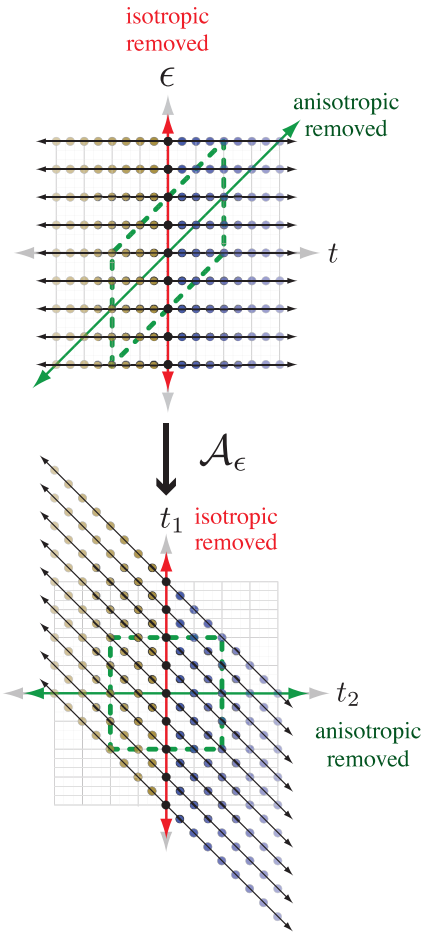

Figure 6: Affine transformation, $\mathcal{A}_\epsilon$, for transforming the 2D PASS signal, $\mathcal{S}(\epsilon, t)$, into a 2D signal that correlates isotropic and anisotropic frequencies, consists of a shear parallel to ϵ, giving a 2D signal with anisotropic frequencies refocused along the t_2 axis and isotropic frequencies refocused along t_1. The green dashed line in the top figure represents the passive affine transformation of the 2D coordinate system to create a time coordinate, t_2, along which the 2D signal is unaffected by the isotropic frequency contributions.

by a scaling of $\varsigma^{(\epsilon^*)} = -1$, as outlined in Fig. 6, and given by

$$\begin{aligned}\begin{bmatrix} t_1 \\ t_2 \end{bmatrix} &= \underbrace{\begin{bmatrix} -1 & 0 \\ 0 & 1 \end{bmatrix}}_{\boldsymbol{S}_{\epsilon^*}} \underbrace{\begin{bmatrix} 1 & -1 \\ 0 & 1 \end{bmatrix}}_{\boldsymbol{K}_\epsilon} \begin{bmatrix} \epsilon \\ t \end{bmatrix} \\ &= \begin{bmatrix} -1 & 1 \\ 0 & 1 \end{bmatrix} \begin{bmatrix} \epsilon \\ t \end{bmatrix},\end{aligned} \tag{22}$$

has been the conventional approach for obtaining a 2D spectrum correlating isotropic and anisotropic frequencies. The original acquisition digital sampling rates, $\Delta\epsilon$ and Δt, after the single shear become $\Delta t_1 = \Delta\epsilon = t_R$ and $\Delta t_2 = \Delta t$, respectively. In Fig. 7 is an example of the application of the single shear to a 2D PASS ^{29}Si signal from Clinoenstatite as a function of the number of steps taken in varying ϵ from zero to one full rotor period. Only after 16 steps does the spectral width in the anisotropic (spinning sideband) dimension have sufficient width. The central idea of this work is that the application of TOP processing, that is, a double shear, can allow one to obtain a 2D spectrum with sufficient spectral width in both the isotropic and anisotropic dimension with significantly fewer steps in the ϵ dimension. This is simply because the application of the TOP transformation to the original digital sampling rates, $\Delta\epsilon$ and Δt, yields transformed sampling rates of $\Delta t_2 = \Delta\epsilon = t_R$ and $\Delta t_1 = \Delta t$, respectively. Thus, a ^{29}Si 2D PASS experiment on Clinoenstatite only needs one step in ϵ when using the double shear (TOP) processing approach to resolve the two $Q^{(2)}$ sites in both dimensions, compared to the 16 steps needed with single shear (conventional) processing approach. This is illustrated in Fig. 8, where the TOP processed 2D PASS signals of Clinoenstatite are presented as a function of the number of steps taken in varying ϵ from zero to one full rotor period. Close examination of the Clinoenstatite 2D PASS spectrum reveals a third additional

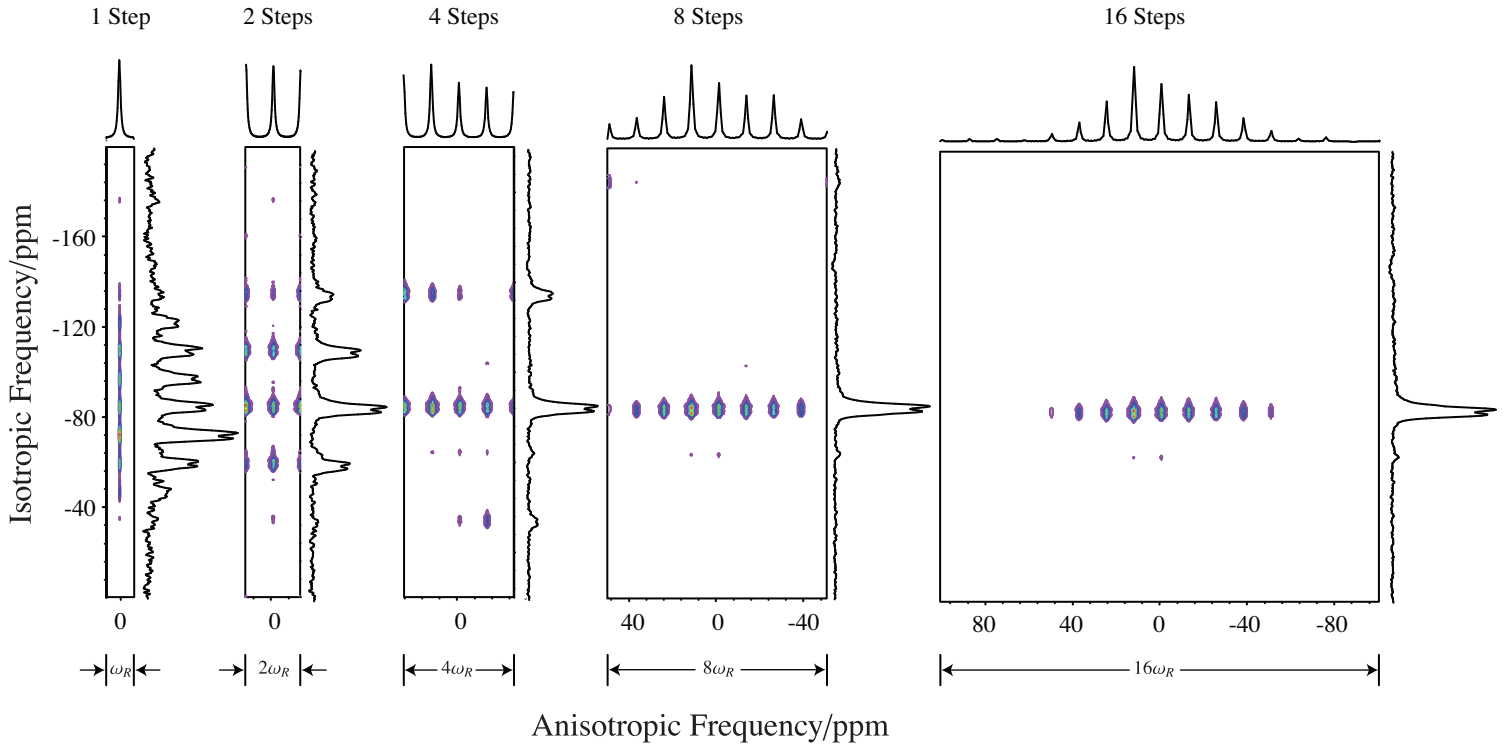

Figure 7: Single shear processing of 2D PASS signal of Clinoenstatite. Isotropic frequencies are referenced to TMS. Contour levels are plotted from 5%-100% in increments of 5% of the maximum intensity.

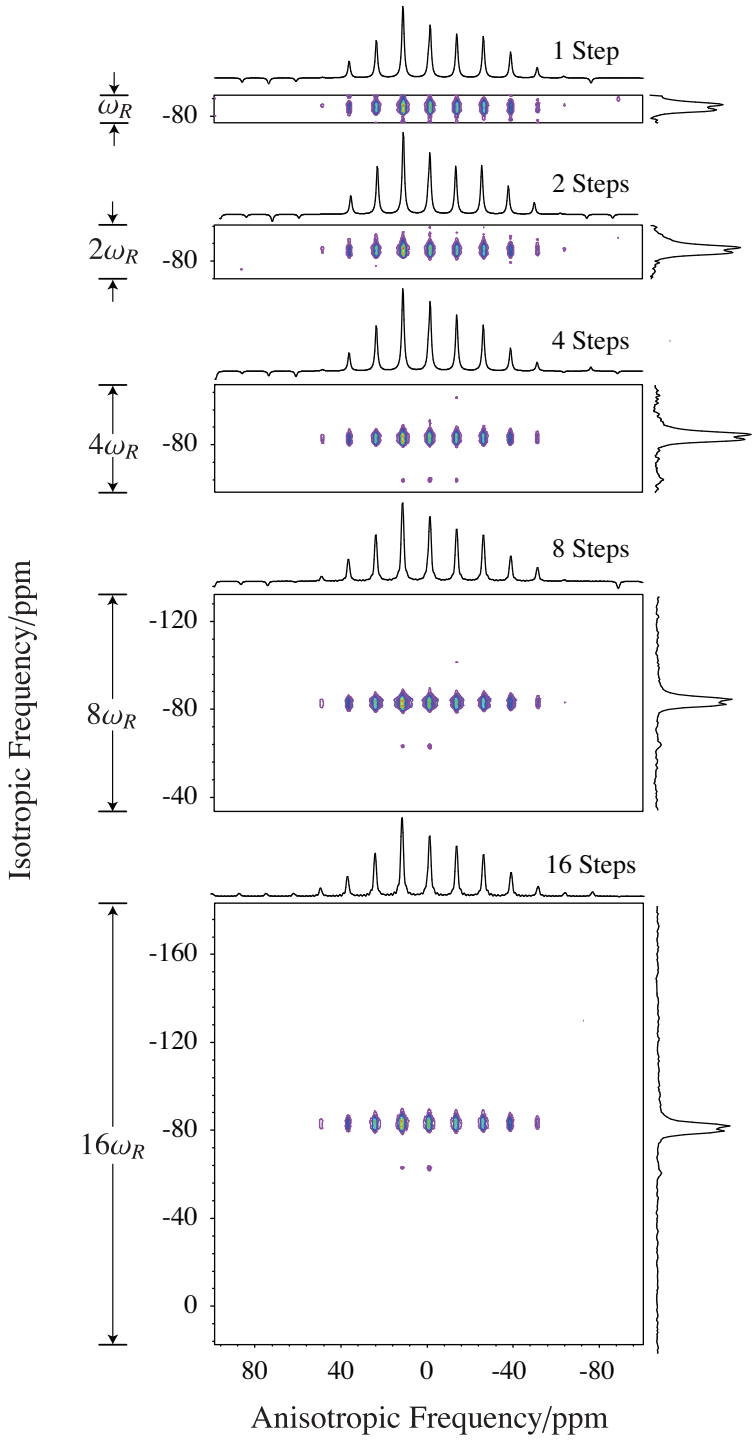

Figure 8: Double shear (TOP) processing of 2D PASS signal of Clinoenstatite. Isotropic frequencies are referenced to TMS. Contour levels are plotted from 5%-100% in increments of 5% of the maximum intensity.

resonance appearing at -63.7 ppm in the isotropic dimension due to a minor impurity of crystalline Forsterite. A proper acquisition of this third site only require 4 steps in the indirect dimension of TOP-PASS, whereas, the conventional 2D PASS experiment would still require 16 steps in the indirect dimension. An additional advantage of the TOP transformation over the single shear transformation is that the spectral width required in the indirect dimension is easily obtained from a high speed MAS spectrum.

When the spectral width in the isotropic dimension is significantly smaller than the spectral width of the anisotropic dimension then the TOP processing can greatly reduce the number of steps required in the ϵ dimension. In contrast, the time savings afforded by TOP processing is less significant as the spectral width of the isotropic dimension approaches that of the anisotropic dimension. To highlight this point, we compare the ^{13}C 2D PASS NMR spectra of L-Histidine[27] processed with the conventional single shear approach, and shown in Fig. 9, with the ^{13}C TOP-PASS spectra, processed with a double shear, and shown in Fig. 10. In this example, the conventionally processed PASS signal required 16 steps when varying ϵ to have sufficient spectral width to prevent aliasing of the carbonyl sideband resonances, whereas the TOP-PASS spectrum required approximately the same number of steps to obtain sufficient spectral width for the full isotropic spectrum.

Finally, it is worth noting that the reason the single shear processing approach fails when applied to the pseudo-2D signal constructed from a Bloch decay MAS signal is because the original digital sampling rates, $\Delta\epsilon$ and Δt, after the single shear become $\Delta t_1 = \Delta\epsilon = t_R$ and $\Delta t_2 = \Delta t$, respectively, and such a sampling rate along t_1, the sideband-only coordinate, simply cannot resolve any spinning sidebands in ω_1.

4. Summary

We have shown that the simple application of the TOP processing approach (i.e., a double shear affine transformation) to 2D PASS signal can significantly reduce the number of measurements needed in the indirect dimension. When applying the TOP transformation to the 2D PASS signal it is the spectral width in the "infinite speed" isotropic dimension that determines the dwell time needed in the indirect dimension. This can lead to significant time savings for systems where the span of the anisotropic lineshapes exceeds the minimum spectral width required for the isotropic dimension. The same approach can be identically applied to signals from the 2D PASS experiment designed for the second-order broadened central transition of half-integer quadrupolar[28, 17].

Acknowledgments

This material is based upon work supported in part by the National Science Foundation. Any opinions, findings and conclusions or recommendations expressed in this material are those of the author(s) and do not necessarily reflect the views of the National Science Foundation (NSF).

[1] G. A. Williams, H. S. Gutowsky, Sample spinning and field modulation effects in nuclear magnetic resonance, Phys. Rev. 104 (1956) 278.

[2] E. R. Andrew, A. Bradbury, R. G. Eades, Removal of dipolar broadening of nuclear magnetic resonance spectra of solids by specimen rotation, Nature 183 (1958) 1802–1803.

[3] I. J. Lowe, Free induction decays of rotating solids, Phys. Rev. Lett. 2 (1959) 285–287.

[4] A. Pines, M. G. Gibby, J. S. Waugh, Proton-enhanced nuclear induction spectroscopy. ^{13}C chemical shielding anisotropy in some organic solids, Chem. Phys. Lett. 15 (1972) 373.

[5] E. O. Stejskal, J. Schaefer, J. S. Waugh, Magic-angle spinning and polarization transfer in proton-enhanced NMR, J. Magn. Reson. 28 (1977) 105–112.

[6] J. Herzfeld, A. E. Berger, Sideband intensities in NMR spectra of samples spinning at the magic angle, J. Chem. Phys. 73 (1980) 6021.

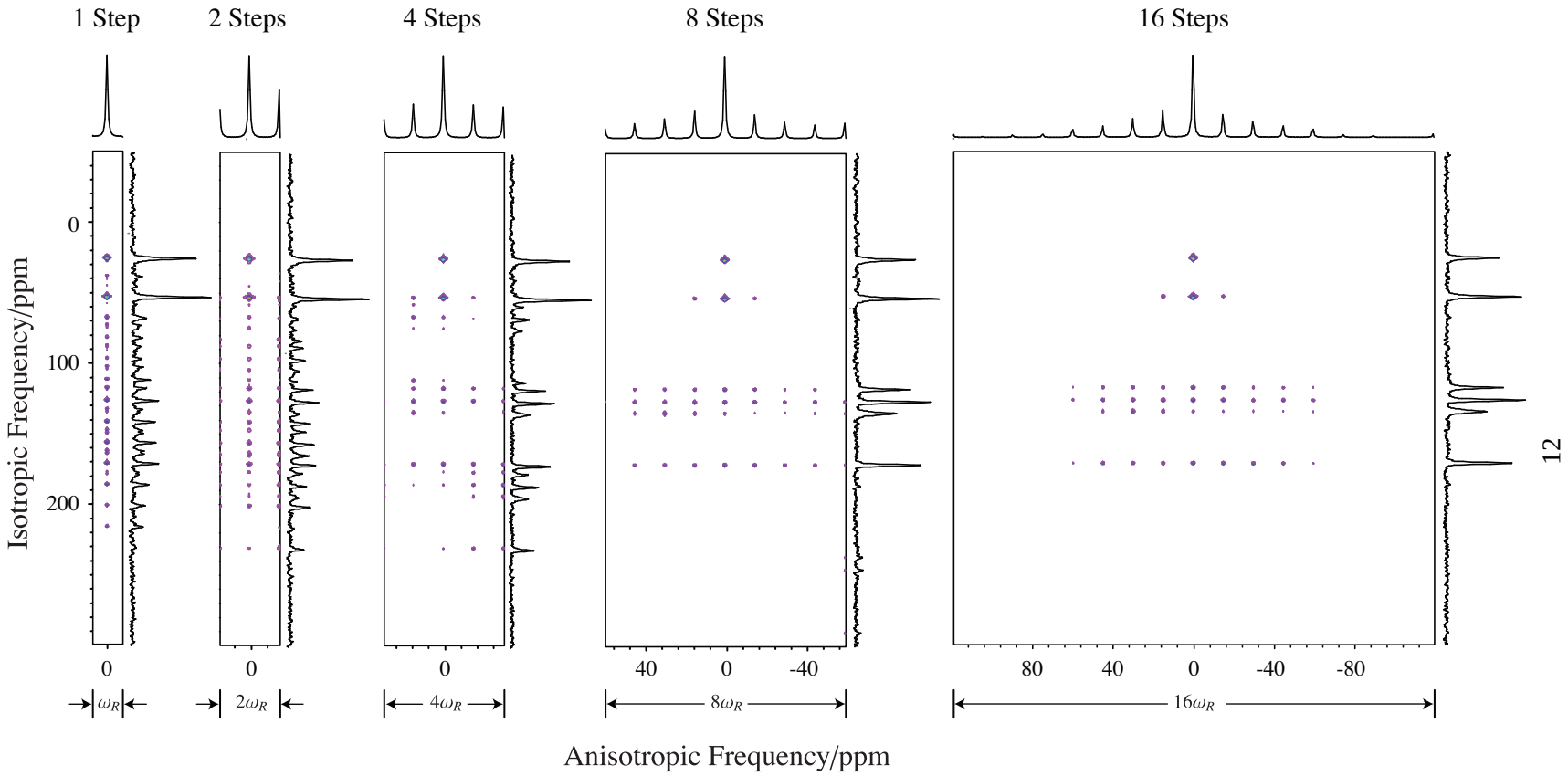

Figure 9: Single shear processing of 2D PASS signal from L-Histidine. Isotropic frequencies are referenced to TMS. Contour levels are plotted from 5%-100% in increments of 5% of the maximum intensity.

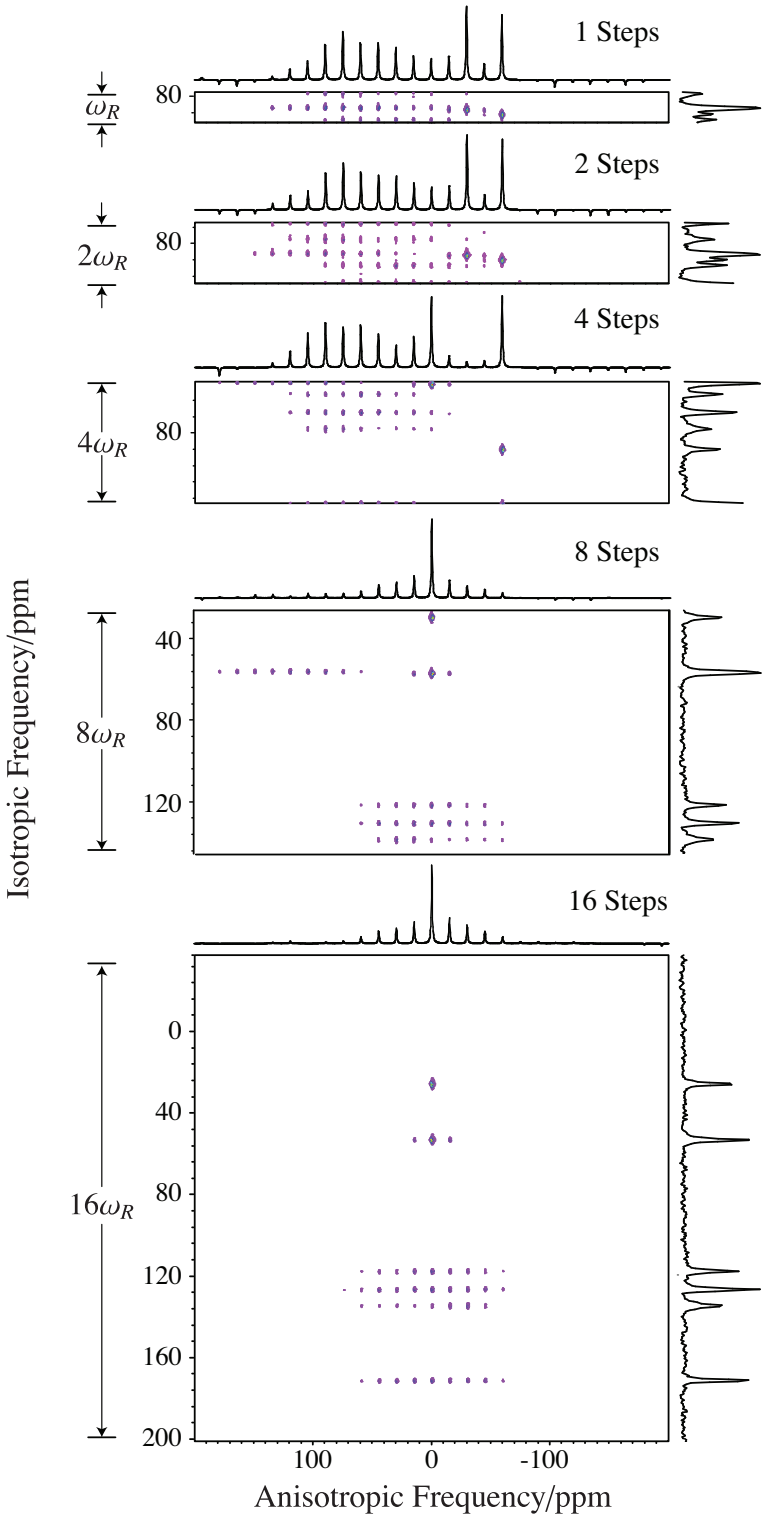

Figure 10: Double shear (TOP) processing of 2D PASS signal from L-Histidine. Isotropic frequencies are referenced to TMS. Contour levels are plotted from 5%-100% in increments of 5% of the maximum intensity.

[7] R. R. Ernst, G. Bodenhausen, A. Wokaun, Principles of Nuclear Magnetic Resonance in One and Two Dimensions, Oxford, Oxford, 1987.

[8] A. Bax, N. M. Szeverenyi, G. E. Maciel, Chemical shift anisotropy in powdered solids studied by 2D FT NMR with flipping of the spinning axis, J. Magn. Reson. 55 (1983) 494.

[9] A. Bax, N. M. Szeverenyi, G. E. Maciel, Correlation of isotropic shifts and chemical shift anisotropies by two-dimensional Fourier-transform magic-angle hopping NMR spectroscopy, J. Magn. Reson. 52 (1983) 147.

[10] T. Terao, T. Fujii, T. Onodera, A. Saika, Switching-angle sample-spinning NMR spectroscopy for obtaining powder-pattern-resolved 2D spectra: Measurements of ^{13}C chemical-shift anisotropies in powdered 3,4-dimethoxybenzaldehyde., Chem. Phys. Lett. 107 (1984) 145.

[11] L. Frydman, G. C. Chingas, Y. K. Lee, P. J. Grandinetti, M. A. Eastman, G. A. Barrall, A. Pines, Variable-angle correlation spectroscopy in solid-state nuclear magnetic resonance, J. Chem. Phys. 97 (7) (1992) 4800–4808.

[12] P. J. Grandinetti, Y. K. Lee, J. H. Baltisberger, B. Q. Sun, A. Pines, Sideband patterns in dynamic-angle spinning NMR, J. Magn. Reson. A 102 (1993) 195.

[13] R. Tycko, G. Dabbagh, P. A. Mirau, Determination of chemical shift anisotropy lineshapes in a two-dimensional magic angle spinning nmr experiment, J. Magn. Reson. 85 (1989) 265.

[14] J. Z. Hu, D. W. Alderman, C. H. Ye, R. J. Pugmire, D. M. Grant, An isotropic chemical shift-chemical shift anisotropy magic-angle slow-spinning 2D NMR experiment, J. Magn. Reson. A 105 (1) (1993) 82–87.

[15] A. C. Kolbert, R. G. Griffin, 2-dimensional resolution of isotropic and anisotropic chemical-shifts in magic-angle spinning NMR, Chem. Phys. Lett. 166 (1) (1990) 87–91.

[16] O. N. Antzutkin, S. C. Shekar, M. H. Levitt, Two-dimensional sideband separation in magic-angle spinning NMR, J. Magn. Reson. A 115 (1995) 7–19.

[17] D. Massiot, V. Montouillout, F. Fayon, P. Florian, C. Bessada, Order-resolved sidebands separation in magic angle spinning NMR of half integer quadrupolar nuclei, Chem. Phys. Lett. 272 (1997) 295–300.

[18] Z. H. Gan, High-resolution chemical-shift and chemical-shift anisotropy correlation in solids using slow magic-angle spinning, J. Am. Chem. Soc. 114 (21) (1992) 8307–8309.

[19] W. T. Dixon, Spinning-sideband-free and spinning-sideband-only NMR spectra in spinning samples, J. Chem. Phys. 77 (1982) 1800.

[20] B. Blümich, P. Blumler, J. Jansen, Presentation of sideband envelopes by two-dimensional one-pulse (TOP) spectroscopy, Solid State NMR 1 (1992) 111–113.

[21] P. Blumler, B. Blümich, J. Jansen, Two-dimensional one-pulse rotational echo spectra, Solid State NMR 3 (1994) 237–240.

[22] D. Massiot, J. Hiet, N. Pellerin, F. Fayon, M. Deschamps, S. Steuernagel, P. J. Grandinetti, Two dimensional one pulse MAS of half-integer quadrupolar nuclei, J. Magn. Reson. 181 (2006) 310–315.

[23] P. J. Grandinetti, J. T. Ash, N. M. Trease, Symmetry pathways in solid-state NMR, Prog. N.M.R. Spect. (2010) in press.

[24] P. Zhang, P. J. Grandinetti, J. F. Stebbins, Anionic species determination in $CaSiO_3$ glass using two-dimensional ^{29}Si NMR, J. Phys. Chem. B 101 (20) (1997) 4004–4008.

[25] M. Davis, D. Kaseman, S. Parvani, K. Sanders, P. Grandinetti, P. Florian, D. Massiot, $Q^{(n)}$-species distribution in K_2O $2SiO_2$ by ^{29}Si Magic Angle Flipping NMR, J. Phys. Chem. A 114 (17) (2010) 5503–5508.

[26] W. T. Dixon, Spinning-sideband-free NMR-spectra, Journal of Magnetic Resonance 44 (1981) 220.

[27] C. Gardiennet-Doucet, X. Assfeld, B. Henry, P. Tekely, Revealing successive steps of deprotonation of l-phosphoserine through ^{13}C and ^{31}P chemical shielding tensor fingerprints, J. Phys. Chem. A 110 (2006) 9137–9144.

[28] W. T. Dixon, Pulse sequence for spinning sideband suppression in spectra of quadrupolar nuclei, Journal of Magnetic Resonance 64 (1985) 64.